Mechanism of CO_2 capture in nanostructured sodium amide encapsulated in porous silica

Tian, Mi; Buchard, Antoine; Wells, Stephen A.; Fang, Yanan; Torrente-Murciano, Laura; Nearchou, Antony; Dong, Zhili; White, Timothy J.; Sartbaeva, Asel; Ting, Valeska P.

DOI:
10.1016/j.surfcoat.2018.06.049

Mechanism of CO_2 capture in nanostructured sodium amide encapsulated in porous silica

Mi Tian[a], Antoine Buchard[b], Stephen Wells[a], Yanan Fang[c], Laura Torrente-Murciano[d], Antony Nearchou[b], Zhili Dong[c], Timothy. J. White[c], Asel Sartbaeva[b*] and Valeska P. Ting[e*]

[a.]Department of Chemical Engineering, University of Bath, Bath BA2 7AY, United Kingdom.

[b.]Department of Chemistry, University of Bath, Bath BA2 7AY, United Kingdom.

[c.]School of Materials Science and Engineering, Nanyang Technological University, Singapore

[d.]Department of Chemical Engineering and Biotechnology, University of Cambridge, Cambridge CB2 3RA, United Kingdom.

[e.]Department of Mechanical Engineering, University of Bristol, Bristol BS8 1TR, United Kingdom.

ABSTRACT

Nanostructured sodium amide encapsulated in a porous silica gel matrix ("$NaNH_2$-SG") was investigated for CO_2 capture and storage by in-situ gravimetric gas sorption. Exposure of $NaNH_2$-SG to CO_2 at 25 ^{0}C and 1 bar pressure resulted in ~ 3.6 wt. % CO_2 uptake over eight sorption/desorption cycles. Over 90% of the CO_2 uptake was non-reversible due to reaction between CO_2 and $NaNH_2$ to form sodium carbamate, as confirmed by ^{13}C and ^{23}Na solid-state NMR. Electronic structure calculations suggest a two-stage reaction process involving initial formation and subsequent rearrangement of the carbamate product. This research confirms the feasibility of sequential reactions of nanoparticles in a porous substrate (Na-SG to $NaNH_2$-SG to Na-carbamate-SG), and of CO_2 capture by $NaNH_2$-SG nanoparticles stabilised by encapsulation within the porous substrate. This encapsulation method could allow further hygroscopic or reactive starting reagents or compounds to be explored for CO_2 capture and long-term storage.

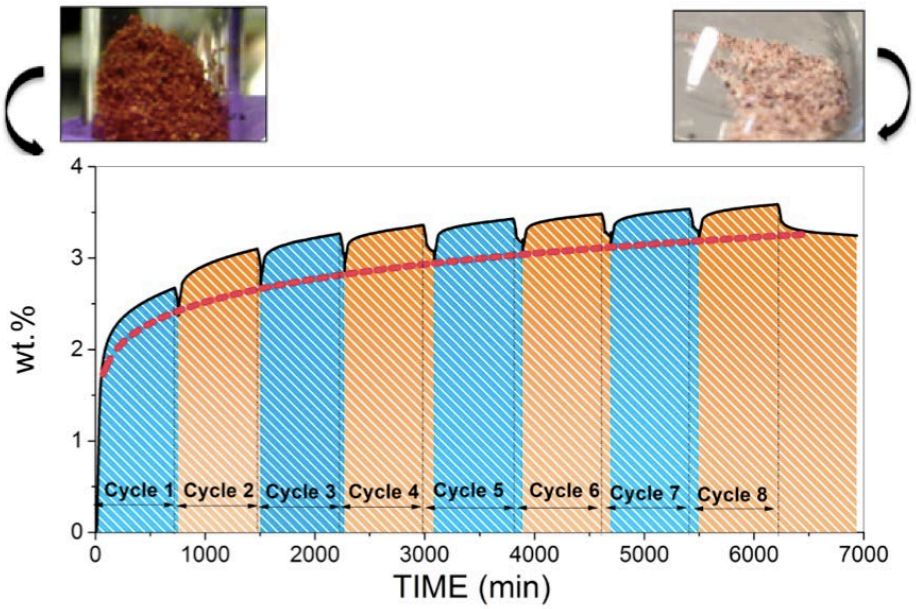

1. INTRODUCTION

Concern over the serious environmental and economic implications of climate change have prompted many countries to commit to lowering of CO_2 emissions.[1, 2] Currently, the majority of anthropogenic atmospheric CO_2 emissions originate from transportation and fossil fuel based power generation. A range of CO_2 capture and storage techniques such as chemical absorption, physical adsorption, cryogenic distillation, and membrane technologies have been explored,[3] for industrial post-combustion CO_2 capture (also known as flue gas scrubbing). Recently, use of alternative solid amine adsorbents have shown promise for CO_2 capture. These materials are prepared through the physical or chemical immobilisation of amines onto solid supports such as activated carbon,[4, 5] zeolites[6, 7] and porous silica.[8-11] As well as amines, solid sodium-based sorbents such as sodium hydroxide and sodium carbonates have been investigated for CO_2 capture.[12, 13] The use of more strongly reactive compounds such as sodium amide has also been proposed, but their chemical instability limits their usefulness. The reactivity of sodium amide with CO_2 opens up possibilities for accessing long-term CO_2 storage, such as is used in mineralisation[14], provided the drawbacks associated with the chemical instability and pyrophoric nature of such compounds can be overcome.

This work examines the interaction of CO_2 with crystalline sodium amide nanoparticles that have been encapsulated in a porous silica matrix. This material, hereafter called $NaNH_2$-SG, enabled the stabilization of the highly reactive sodium amide compound, potentially making it useful as a solid CO_2 sorbent. The feasibility of CO_2 capture and storage using this $NaNH_2$-SG material was then investigated using experimental and computational approaches. This work demonstrates the feasibility of successive reactions (Na-SG to

$NaNH_2$-SG to Na-carbamate-SG) in nanoparticles encapsulated within a porous silica matrix.

2. EXPERIMENTAL METHODS

2.1.Preparation of the $NaNH_2$-SG

$NaNH_2$-SG was prepared[15] by saturating a commercially available sodium-loaded silica gel material (Na-SG) with ammonia.[16] The commercially-available starting material (sodium encapsulated in a porous silica gel, denoted as Na-SG, 37 wt. % Na),[16-18] is produced by agitation of a mixture of molten sodium and silica gel. As synthesized, the Na-SG is a coarse black powder with nano-sized sodium particles dispersed within the pores of a silica matrix, the pore diameters being up to 150 nm[17]. ~ 0.5g Na-SG was exposed to gaseous anhydrous ammonia in a differential tubular reactor at 338 K for over 20 h, upon which the material changed colour from black to brown due to the *in-situ* formation of a sodium amide contained in the pores of the silica matrix; this material is henceforth denoted as $NaNH_2$-SG.[15] The degree of conversion of Na to $NaNH_2$ was calculated using *Equation 1* and *Equation 2* to be approximately 24 ± 3 % by mole, the variance being estimated from five separately produced samples.

$$w_{Na} = w_{Na-SG} \times 37\ \% \qquad \textit{Equation 1}$$

$$Conversion = \frac{\frac{w_t - w_{Na-SG}}{M_{NH_2}}}{\frac{w_{Na}}{M_{Na}}} \times 100\ \% \qquad \textit{Equation 2}$$

where w_{Na} is the weight of Na in the Na-SG, w_{Na-SG} is the total weight of Na-SG starting material, w_t is the weight of the synthesized sample of $NaNH_2$-SG, M_{Na} is the molar mass of Na and M_{NH_2} is the molar mass of NH_2.

A similar process (using hydrogen as the reactant gas) was used in previously by the authors to synthesize an encapsulated sodium hydride, NaH-SG.[19] The resulting encapsulated $NaNH_2$-SG, as with the NaH-SG[19], did not display any pyrophoricity. Furthermore, it can be observed visually that the encapsulated $NaNH_2$-SG material oxidises/hydrolyses at a lower rate compared to the bulk Na amide, which would burst into flames in air. The oxidation of the $NaNH_2$-SG occurs more slowly (over several minutes) and is characterized by an irreversible colour change from brown to white.

2.2.Structural characterization

Scanning Electron Microscopy (SEM) backscattered imaging and Energy Dispersive X-ray Spectroscopic (EDS) analyses were carried out with a JSM-7600F field emission scanning electron microscope (FESEM). High Resolution Transmission Electron Microscopy (HRTEM) analysis was carried out on a JEOL JEM-2100F equipped with a 200 kV field emission gun and integrated with Energy Dispersive X-ray Spectrometry (EDS) on samples suspended in ethanol and deposited on holey-carbon grids. Particle size distributions were determined from TEM images using ImageJ software.

The specific surface areas of the SG and $NaNH_2$-SG after CO_2 sorption were obtained using multipoint BET analysis applied to N_2 sorption data collected on a Micromeritics 3Flex volumetric gas sorption analyser at 77 K in the relative pressure (P/P_0) range 0.05 - 0.3. The samples were dried at 60 ^{0}C for 8 h in the vacuum oven and then outgassed *in situ* under

dynamic vacuum (10^{-7} mbar) at 60 ^{0}C for 8 h on the 3Flex prior to N_2 gas sorption measurement at 77 K. Since the pore structure of the silica gel has been well-characterized previously, full N_2 adsorption-desorption isotherms were not collected in this study.

Solid-state NMR spectra (^{13}C and ^{23}Na) were obtained at the EPSRC UK National Solid-State NMR Service at Durham, on ~100 mg samples of $NaNH_2$-SG after exposure to 1 bar CO_2. Measurements were taken on a VNMRS 400 for both nuclei. For the ^{13}C-NMR, frequencies of 100.562 MHz and 50.32 MHz were used for cross polarized (CP) and magic angle spinning (MAS) respectively. Neat trimethylsilane was used as a reference. The ^{23}Na-NMR was recorded with a frequency of 105.784 MHz using MAS, in direct excitation mode without ^{1}H decoupling. For a reference, 1 mole of aqueous sodium chloride was used.

^{1}H NMR and ^{13}C NMR were also used to identify the reactant products after exposure of the $NaNH_2$-SG to CO_2. The $NaNH_2$-SG after CO_2 cycling was analysed by fully quenching the sample with D_2O, and analysing the supernatant by NMR.

2.3.CO_2 sorption procedures

In-situ CO_2 sorption experiments were performed on a Hiden Isochema Intelligent Gravimetric Analyser (IGA). All sample handling was done under an inert N_2 atmosphere (BOC 99.998 % purity). ~100 mg of $NaNH_2$-SG was degassed prior to analysis under high (3 x 10^{-6} mbar) vacuum at 80 °C until a stable dry weight was reached (~12 h). The temperature of the reactor chamber was controlled by a R4 refrigerated bath, Grant Instruments at 25 ^{0}C. CO_2 gas (BOC, 99.998 % purity) was subsequently introduced at 25 ^{0}C at a rate of 30 mbar min^{-1} to a pressure of 1 bar, with the final pressure maintained for a minimum of 720

minutes to allow the system to reach equilibrium. To study the behaviour of the system under cycling, the adsorbent was exposed to high vacuum in situ at 25 ^{0}C after every sorption cycle, until no further decrease in weight was observed (approx. 600 mins), before starting the sorption step of the next cycle. Sorption was expressed in weight %, using the initial weight of the dry material (after degassing) as the basis.

Control experiments were performed using a ~100 mg sample of pure silica gel (SG) (Sigma Aldrich, Davisil®, Grade 646, size 150 Å, 35-60 mesh), in order to distinguish between CO_2 adsorption onto the silica framework and reactions with the contained nanoparticles of sodium amide. The SG control sample was dried overnight in a vacuum oven at 150 ^{o}C prior to loading onto the IGA microbalance under inert conditions. The CO_2 adsorption and desorption isotherm of the pure SG was measured on the IGA up to a pressure of 1 bar at 25 ^{0}C. The reaction of CO_2 with pure $NaNH_2$ was not performed in this study due to the known risk of producing explosive compounds.

2.4.Molecular simulation

Density Functional Theory (DFT) calculations to investigate a proposed reaction pathway between CO_2 and sodium amide were carried out in the gas phase, with a default pressure (1 bar) and temperature (298.15 K), using the M06-2X functional and the 6-311++G(d,p) split-valence triple ζ basis set with polarisation and diffuse functions. The basis set was selected to account for potential anions and non-bonding interactions. The M06-2X functional is one of the hybrid meta-generalised-gradient-approximation (hybrid meta-GGAs) exchange-correlation functionals developed by Truhlar *et al.[20]* M06-2X includes 54% of

Hatree-Focke exchange, and has been parameterised for non-metals and is recommended for application in main group thermochemistry, kinetics and the study of non-covalent interactions. [21] All geometries were fully optimised without symmetry or geometry constraints, but only the most stable conformational isomers are reported for all intermediates. The nature of all the stationary points as minima or transition states was verified by calculations of the vibrational frequency spectrum: local minima are characterised by the absence of an imaginary mode, whereas transition states were characterized by precisely one imaginary mode corresponding to the intended reaction. These were augmented by an intrinsic reaction coordinate (IRC) calculation to confirm reaction identity. [21-23] Free energies were calculated within the harmonic approximation for vibrational frequencies. All modelling was carried out using the Gaussian09 suite of codes.[24] Full coordinates for all stationary points, together with computed free enthalpies and vibrational frequency data, are available via the corresponding Gaussian 09 output files, stored in the digital repository DOI: 10.6084/m9.figshare.3081643.

3. RESULTS AND DISCUSSION

3.1.Sorption of CO_2 in $NaNH_2$-SG-CO_2 and SG-CO_2 systems

The interactions of CO_2 with the SG and the synthesised $NaNH_2$-SG material were investigated via gravimetric gas sorption analysis and showed noticeably different sorption behaviours. Adsorption of CO_2 at and 1 bar on the bare SG material

resulted in an almost linear CO_2 sorption isotherm characteristic of weak physical adsorption, with a CO_2 loading of ~1.7 wt. %. This adsorption was almost fully reversible, with the adsorbed gas quickly removed under high vacuum at 25 ^{0}C (**Figure 1**). The corresponding measurement of CO_2 on $NaNH_2$-SG at 25 ^{0}C resulted in a Type I isotherm with a maximum uptake of ~ 2.7 wt. % at 1 bar and incomplete desorption, showing a much stronger interaction with the CO_2 as a result of the encapsulated $NaNH_2$.

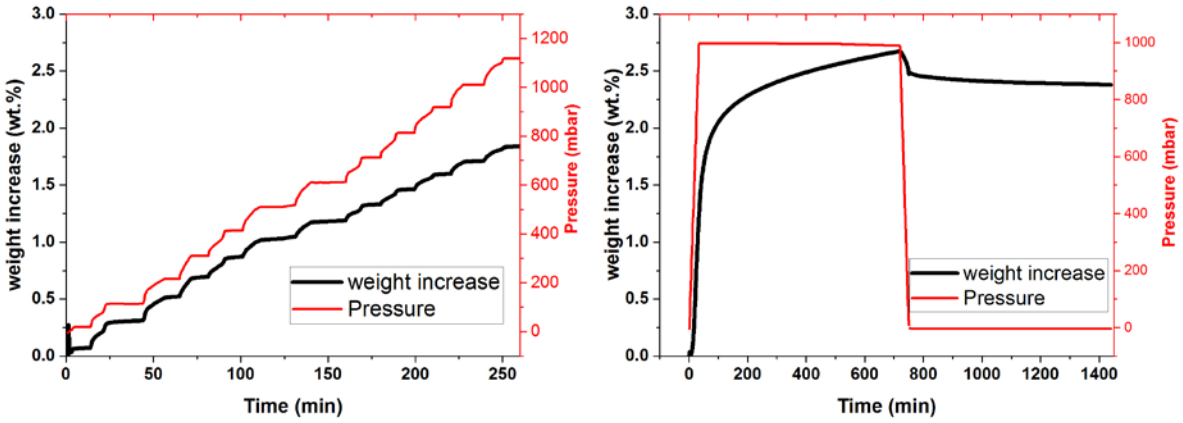

Figure 2: (left) Kinetics of CO_2 adsorption on the pure SG at 25 ^{0}C up to 1.2 bar as measured by gravimetric gas sorption; (right) Gravimetric CO_2 sorption at 1 bar at 25 ^{0}C on $NaNH_2$-SG, and desorption under vacuum. showing high CO_2 retention even upon application of high vacuum (at ~720 mins). The black lines in each plot represent weight change (wt%) and the red lines indicate CO_2 pressure in mbar.

The CO_2 sorption on the $NaNH_2$-SG as a function of time was investigated to determine adsorption kinetics. Figure 2 shows the kinetics of CO_2 adsorption on the SG at 25 ^{0}C up to 1.1 bar, indicating that the entire isotherm took ~260 min over 13 steps and equilibrated over 20 min for each dosing step. The CO_2 loading of ~ 2.7 wt. % on $NaNH_2$-SG at 1 bar agreed with the equilibrium adsorption capacity shown in Figure 1 but illustrates the significant difference in equilibration times between the SG and $NaNH_2$-SG materials. The CO_2 uptake in the $NaNH_2$-SG was largely irreversible under high vacuum at 25 ^{0}C and characteristic of strong-

er sorption interactions compared to the SG substrate which showed almost complete reversibility with decreased CO_2 gas pressure (see Figure 1). Indeed, only 0.3 wt. % reversibly desorbed over 600 min in the $NaNH_2$-SG at high vacuum (Figure 2). This largely irreversible uptake demonstrates that the dominant mechanism in the case of the $NaNH_2$-SG was not pure physisorption onto the porous silica, but either the result of strong binding (chemisorption) of molecular CO_2 to the sodium amide in the pores of the silica matrix, or a chemical reaction between the amide and the CO_2, as would be expected for a non-encapsulated amine/amide. In the case of the $NaNH_2$-SG the CO_2 uptake had not reached a plateau even after 720 minutes, even though the equilibration times used here would typically be ample for physical adsorption of CO_2 (as exemplified by the isotherm of CO_2 on SG in Figure 2).

To examine the stability and further investigate the CO_2 saturation of $NaNH_2$-SG, the material was cycled between 1 bar CO_2 pressure and high vacuum over 8 cycles at 25 ^{0}C. This cycling resulted in an irreversible weight increase after each sorption cycle, accompanied by a smaller reversible component, to a saturation limit of ~3.6 wt. % by the 8th cycle (Figure 3). The total weight increase was concluded to result from two effects: ~3.3 wt. % weight gain from the irreversible interaction between CO_2 and $NaNH_2$ (the dotted line in Figure 3) and ~0.3 wt. % from the reversible physisorption of CO_2 onto the porous silica. The irreversibility of the strong binding would prevent the use of the solid material for pressure-swing adsorption/desorption, but is a valuable feature for long-term CO_2 capture and storage.

During cycling, the $NaNH_2$-SG changed colour from dark brown to light pink while retaining its granular morphology, indicating a reaction between the CO_2 and the encapsulated sodium amide (see Figure 3).

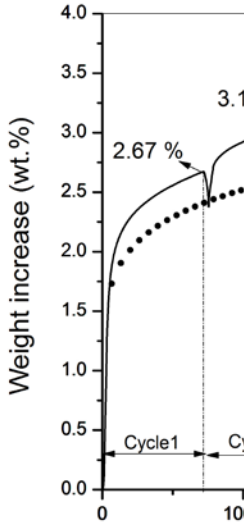

Figure 3: CO_2 capture cycles of $NaNH_2$-SG at 25^{0}C under CO_2 pressure, alternating between 1 bar and high vacuum.

Srivastava *et al*. described the reaction (1), [26]

$$CO_2 + NH_2^- \rightarrow NH_2COO^- \qquad (1)$$

as an intermediate during the formation of ammonium carbamate from ammonia and carbon dioxide (reaction 2):

$$2NH_3 + CO_2 \rightarrow NH_2COO^-NH_4^+ \qquad (2)$$

The colour change accompanying the conversion of $NaNH_2$ to sodium carbamate encapsulated in the silica matrix can be attributed to the reaction (3):

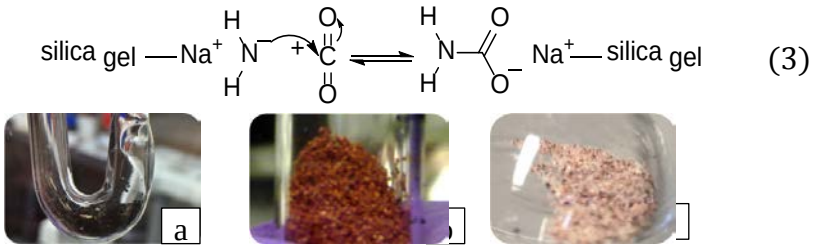

Figure 5 (a) Na-SG (black powder), (b) $NaNH_2$-SG, and (c) sodium carbamate in SG.

From Figure 3, the amount of weakly adsorbed and partially reversible CO_2 uptake for the $NaNH_2$-SG remained relatively constant (~0.3 wt. %) during cycling at 25 ^{0}C, while the differential weight gains due to the irreversible component gradually decreased with number of cycles as the $NaNH_2$ became saturated with CO_2.

After the 8th cycle, the sample was heated under vacuum to 80 °C for 120 min, and showed removal of ~0.6 wt. % of the weakly bonded CO_2.

TEM images of the $NaNH_2$-SG after eight CO_2 sorption cycles showed the persistence of distinct, isolated nanoparticles dispersed within the silica matrix (*Figure 5*). In addition, ImageJ analysis of the TEM images showed a normal distribution of particle sizes over the range of 10 – 90 nm with mean diameter of 46 $\pm$ 0.8 nm, consistent with previous

reports.[15, 19] Scanning electron microscopy (SEM) after CO_2 uptake showed large openings or cavities on the surface of the porous silica (*Figure 5* c and d). Taken together, these results confirm that nanostructured crystalline sodium compounds were encapsulated within the porous silica. The morphological similarity observed in this case to those seen during the formation of NaH-SG and $NaNH_2$-SG[15, 19] indicates CO_2 capture proceeds without disrupting the silica matrix.

The rapid CO_2 uptake in each cycle is consistent with initial adsorption between CO_2 and $NaNH_2$-SG prior to the irreversible strong interaction. However, the observed weight gain of 3.3 wt. % seen for the $NaNH_2$-SG is much lower than the theoretical weight gain predicted for carbamate formation (15.2 wt. %, based on the 24 % conversion of Na to $NaNH_2$, as measured gravimetrically). The presence of the Na-NH_2 groups already coordinated to CO_2 groups could be responsible for hindering the diffusion and further conversion of CO_2 into the pores. Thus, the formation of the stronger interactions between the Na-NH_2 and the CO_2 may be diffusion limited once the $NaNH_2$ at the entrance of the pores is saturated. The larger measured BET surface area of the pure SG (330 $m^2\ g^{-1}$), compared to the $NaNH_2$-SG (228 $m^2\ g^{-1}$) accounts for the slightly higher wt. % of reversible physisorption of CO_2 on the SG substrate while the smaller surface area of the sodium carbamate-SG can be attributed to occlusion of pores by the nanostructured sodium compounds. To investigate this further, NMR and molecular modelling were employed to identify potential reaction products.

3.2.Molecular simulations of reaction pathway

DFT calculations in the gas phase are able to provide information about the potential reaction products, although it is important to note that it does not model the effect of the encapsulation in $NaNH_2$-SG. The complex nanostructure of the material and the amorphous SG structure make it impractical to carry out solid-phase calculations using a periodic unit cell.

The Gibbs free energy profile of the most favourable reaction shows the reaction of CO_2 +$NaNH_2$ proceeds in two thermodynamically favoured steps (*Figure 6*). The first step is the nucleophilic attack of the nitrogen atom of $NaNH_2$ on the electrophilic carbon atom of carbon dioxide ($\Delta G = -25.6$ kcal mol^{-1}), Figure 6. The second step is the transfer of the sodium atom from nitrogen to the oxygen of the newly formed carbamate species ($\Delta G = -15.8$ kcal mol^{-1}). Limiting energy barriers of $\Delta G = +2.3$ and $+3.0$ kcal mol^{-1} for the nucleophilic attack and the sodium transfer steps respectively are low enough for the reaction to proceed readily at 25 ^{0}C. All transition states were characterised by normal coordinate analyses, revealing precisely one imaginary mode corresponding to the intended reaction. In both cases, this was augmented by intrinsic reaction coordinate (IRC) calculations (for $TS_{1\text{-}2}$, the flat energy surface limited the exploration to one direction), which also confirmed the identity of the reaction (see *Figure 7* and *Figure 8*). The overall ΔG of the reaction is calculated to be -41.4 kcal mol^{-1} at 298 K. The formation of sodium carbamate from carbon dioxide and

sodium amide is therefore strongly thermodynamically favoured, and is consistent with the irreversible CO_2 uptake of the $NaNH_2$-SG observed experimentally. While the encapsulation effect is not considered in the calculations (*vide supra*), it is logical that, due to the effects of increased local reactant concentration resulting from CO_2 excess adsorption, encapsulation would likely further favour the reaction of sodium amide with CO_2 both kinetically and thermodynamically.

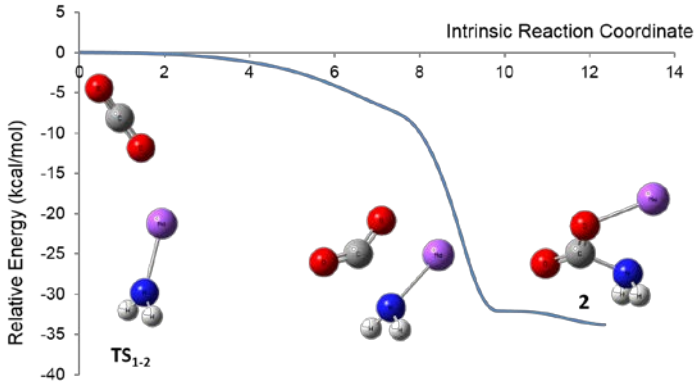

Figure 7: Computed intrinsic reaction coordinates for transition state TS_{1-2} showing the nucleophilic attack of sodium amide on carbon dioxide.

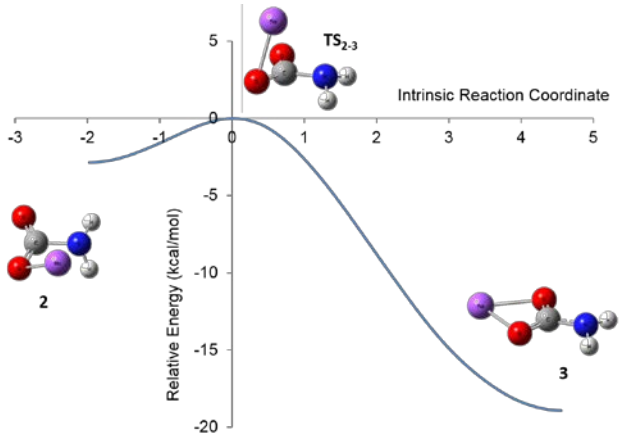

Figure 8: Computed intrinsic reaction coordinate for transition state TS2-3 showing rotation of the sodium atom from the nitrogen atom to the oxygen atoms of the carbamate 3.

3.3.NMR analysis of reaction products

To confirm the chemical conversion of CO_2 into carbamate, solid state ^{13}C-NMR was carried out on a $NaNH_2$-SG sample exposed to 1 bar CO_2. A spectrum recorded in cross polarisation (CP) mode showed two distinct signals at 164.69 ppm and 170 ppm (*Figure 9* a). Both of those signals lie in the carbamate region of the spectrum. To give a CP signal those species must have a reasonably close relationship to ^{1}H. The ^{23}Na SS NMR spectrum showed two signals at 4.63 ppm and 6.43 ppm (*Figure 9* b), which can be assigned to two different environments of sodium in the vicinity of carbamate and could feasibly correspond to states 2 and 3 of the DFT calculations.

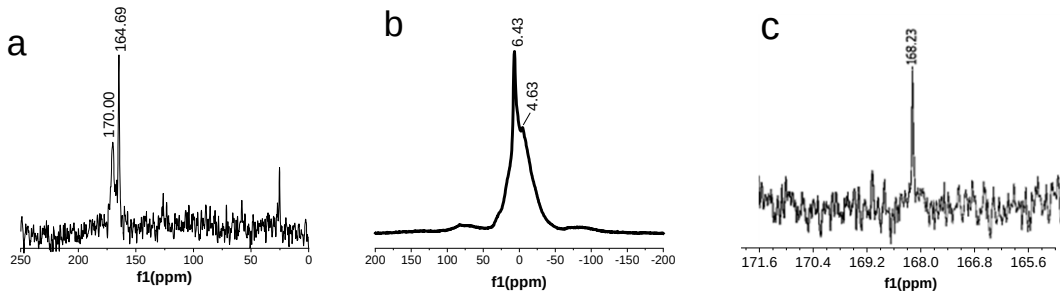

Figure 9: (a) CP Solid State ^{13}C-NMR spectrum of $NaNH_2$-SG-CO_2. (Peak around 25ppm is contamination due to finger grease); (b) Solid State ^{23}Na-NMR spectrum of $NaNH_2$-SG-CO_2; (c) ^{13}C NMR spectrum in D_2O of $NaNH_2$-SG-CO_2 after liquid extraction.

In order to further investigate the formation and persistence of carbamate species in our material after CO_2 exposure, the CO_2-loaded $NaNH_2$-SG was opened, fully quenched with D_2O, and the supernatant obtained analysed by NMR. The ^{1}H NMR spectrum is essentially featureless with no observable peaks. The ^{13}C NMR spectrum displayed a sole singlet at 168.23 ppm (see *Figure 9* c). The direct reaction of sodium amide with water would only produce sodium hydroxide and water with no carbon-containing species. The signal ob-

served could correspond to either a carbamate or a carbonate species. Gottlieb *et al.* [25] reported ^{13}C NMR chemical shifts of 168.88 ppm for sodium carbonate and 161.08 ppm for sodium hydrogen carbonate in D_2O, while 161.97 ppm has been reported for ammonium carbamate in D_2O.[26] Based on ^{13}C NMR, the compound extracted with D_2O could be a carbamate or a mixed sodium/ammonium carbonate species, formed by hydration of sodium carbamate (see Scheme 1).

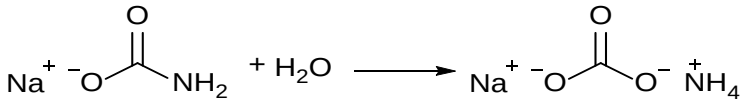

Scheme 1: Potential hydration reaction of sodium carbamate species leading to mixed sodium/ammonium carbonate species**.**

Preliminary DFT calculations to investigate the latter proposed reaction, using the same level of theory as before but augmented with a self-consistent-reaction-cavity continuum solvation model to account for the solvent water (protocol SCRF=(cpcm, solvent=water)) found in Scheme 1, is slightly unfavourable thermodynamically ($\Delta G = +3.1$ kcal mol^{-1} at 298 K). However, given the uncertainties involved in the calculation and the small ΔG, the reaction cannot be ruled out. While further work is needed to establish the exact nature of the species extracted from $NaNH_2$-SG-CO_2, it is apparent that $NaNH_2$-SG does react with CO_2, with the calculations supporting the evidence for formation of the carbamate species from the experimental measurements.

4. CONCLUSION

The interaction of carbon dioxide with a nanostructured sodium amide contained within silica gel was investigated as a potential method of carbon capture and storage. The materi-

al contained nano-sized particles of crystalline sodium compounds with an average particle size of 46 $\pm$ 0.8 nm dispersed within the porous silica matrix. The $NaNH_2$-SG displayed the ability to capture up to 3.6 wt. % CO_2 at 25 ^{0}C. Cycling CO_2 uptake on $NaNH_2$-SG showed that compared to SG, there is a small reversible physical CO_2 adsorption and a larger irreversible uptake of ~3.3 wt. % which was attributed to a chemical reaction of the CO_2 with $NaNH_2$-SG. The irreversible uptake, retained under high vacuum, would prevent the use of the solid material for pressure-swing adsorption/desorption, but is a potentially valuable feature for long-term CO_2 capture and storage.

The DFT modelling suggests conversion of $NaNH_2$ to sodium carbamate, with SSNMR providing experimental evidence for formation of a sodium carbamate species. The demonstration of successive reactions of a solid reagent within the porous silica gel framework (Na-SG → $NaNH_2$-SG → sodium carbamate-SG) opens up the possibility of encapsulating further highly reactive compounds into porous materials for solid CO_2 capture. In addition, it highlights the potential for the encapsulation of hygroscopic or reactive starting materials within frameworks to stabilise and enable otherwise unfavourable or unsafe reactions. The measured irreversible CO_2 uptake of ~3.3 wt% is notably less than what would be expected for a stoichiometric conversion to the carbamate. This indicates that while the encapsulation may allow use of these reactive $NaNH_2$ species, the pore sizes or distributions of the active species may need to be more closely controlled to manage steric factors limiting the access to the reactive sites. If the degree of uptake could be increased closer to the stoichiometric value (~15 wt. % for this material) and long term retention could be confirmed,

carbon capture in a porous reactive solid may be a useful complement to promising but geographically restricted approaches such as mineralization[14].

AUTHOR INFORMATION

Corresponding Authors

*Valeska P. Ting: Department of Mechanical Engineering, University of Bristol, Bristol BS8 1TR, United Kingdom.. E-mail:v.ting@bristol.ac.uk

*Asel Sartbaeva: Department of Chemistry, University of Bath, Bath BA2 7AY, United Kingdom, United Kingdom. E-mail: a.sartbaeva@bath.ac.uk

Funding Sources

The Royal Society for funding for AS via a URF, Roger and Sue Whorrod for funding and the EPSRC NSCCS (chem826) for computing resources for AB and for funding for VT (EP/R01650X/1), the ERC "GROWMOF" project (PI: Prof. Tina Duren, ERC grant No. 648283) for funding for SAW, the University of Bath for funding for VPT via the award of a Prize Research Fellowship, and the H_2FC SUPERGEN Hub (EP/E040071/1) for funding for MT.

ACKNOWLEDGMENTS

The Authors thank Andrew Physick for helping with initial measurements.

REFERENCES

[1] U.S. Greenhouse Gas Inventory Report: 1990-2013, United Nations Framework Convention on Climate Change (UNFCCC)2014.

[2] N. Sun, Z. Tang, W. Wei, C.E. Snape, Y. Sun, Solid Adsorbents for Low Temperature CO_2 Capture with Low Energy Penalties Leading to More Effective Integrated Solutions for Power Generation and Industrial Processes, Frontiers in Energy Research, 3 (2015).

[3] M. Kianpour, M.A. Sobati, S. Shahhosseini, Experimental and modeling of carbon dioxicde capture by dry sodium hydroxide carbonation, Chemical Engineering Research and Design, 90 (2012) 2041-2050.

[4] D. Bezerra, F. Da Silva, P. De Moura, K. Sapag, R. Vieira, E. Rodriguez-Castellon, D. De Azevedo, Adsorption of CO_2 on amine-grafted activated carbon, Adsorption Science and Technology, 32 (2014) 141-151.

[5] M. Keramati, A.A. Ghoreyshi, Improving CO_2 adsorption onto activated carbon through functionalization by chitosan and triethylenetetramine, Physica E: Low-Dimensional Systems and Nanostructures, 57 (2014) 161-168.

[6] D.P. Bezerra, R.S. Oliveira, R.S. Vieira, C.L. Cavalcante, D.C.S. Azevedo, Adsorption of CO_2 on nitrogen-enriched activated carbon and zeolite 13X, Adsorption, 17 (2011) 235-246.

[7] F. Su, C. Lu, S.C. Kuo, W. Zeng, Adsorption of CO_2 on amine-functionalized y-type zeolites, Energy and Fuels, 24 (2010) 1441-1448.

[8] Y. Du, Z. Du, W. Zou, H. Li, J. Mi, C. Zhang, Carbon dioxide adsorbent based on rich amines loaded nano-silica, Journal of Colloid and Interface Science, 409 (2013) 123-128.

[9] W. Klinthong, K.J. Chao, C.S. Tan, CO_2 capture by as-synthesized amine-functionalized MCM-41 prepared through direct synthesis under basic condition, Industrial and Engineering Chemistry Research, 52 (2013) 9834-9842.

[10] Y. Le, D. Guo, B. Cheng, J. Yu, Amine-functionalized monodispersed porous silica microspheres with enhanced CO_2 adsorption performance and good cyclic stability, Journal of Colloid and Interface Science, 408 (2013) 173-180.

[11] X. Zhang, H. Qin, X. Zheng, W. Wu, Development of efficient amine-modified mesoporous silica SBA-15 for CO_2 capture, Materials Research Bulletin, 48 (2013) 3981-3986.

[12] B. Dutcher, M. Fan, B. Leonard, Use of multifunctional nanoporous $TiO(OH)_2$ for catalytic $NaHCO_3$ decomposition-eventually for $Na_2CO_3/NaHCO_3$ based CO_2 separation technology, Separation and Purification Technology, 80 (2011) 364-374.

[13] Y. Liang, D.P. Harrison, R.P. Gupta, D.A. Green, W.J. McMichael, Carbon dioxide capture using dry sodium-based sorbents, Energy and Fuels, 18 (2004) 569-575.

[14] J.M. Matter, M. Stute, S.O. Snaebjornsdottir, E.H. Oelkers, S.R. Gislason, E.S. Aradottir, B. Sigfusson, I. Gunnarsson, H. Sigurdardottir, E. Gunnlaugsson, G. Axelsson, H.A. Alfredsson, D. Wolff-Boenisch, K. Mesfin, D.F.D. Taya, J. Hall, K. Dideriksen, W.S. Broecker, Rapid carbon mineralization for permanent disposal of anthropogenic carbon dioxide emissions, Science, 352 (2016) 1312-1314.

[15] A.D. Ogilvie, J.W. Makepeace, K. Hore, A.J. Ramirez-Cuesta, D.C. Apperley, J.M. Mitchels, P.P. Edwards, A. Sartbaeva, Catalyst-free synthesis of sodium amide nanoparticles encapsulated in silica gel, Chemical Physics, 427 (2013) 61-65.

[16] M. Shatnawi, G. Paglia, J.L. Dye, K.C. Cram, M. Lefenfeld, S.J.L. Billinge, Structures of Alkali Metals in Silica Gel Nanopores: New Materials for Chemical Reductions and Hydrogen Production, Journal of the American Chemical Society, 129 (2007) 1386-1392.

[17] J.L. Dye, P. Nandi, J.E. Jackson, M. Lefenfeld, P.A. Bentley, B.M. Dunyak, F.E. Kwarcinski, C.M. Spencer, T.N. Lindman, P. Lambert, P.K. Jacobson, M.Y. Redko, Nano-Structures and Interactions of Alkali Metals within Silica Gel, Chemistry of Materials, 23 (2011) 2388-2397.

[18] J.L. Dye, K.D. Cram, S.A. Urbin, M.Y. Redko, J.E. Jackson, M. Lefenfeld, Alkali Metals Plus Silica Gel: Powerful Reducing Agents and Convenient Hydrogen Sources, Journal of the American Chemical Society, 127 (2005) 9338-9339.

[19] A. Sartbaeva, S.A. Wells, M. Sommariva, M.J.T. Lodge, M.O. Jones, A.J. Ramirez-Cuesta, G. Li, P.P. Edwards, Formation of Crystalline Sodium Hydride Nanoparticles Encapsulated Within an Amorphous Framework, Journal of Cluster Science, 21 (2010) 543-549.

[20] Y. Zhao, D.G. Truhlar, The M06 suite of density functionals for main group thermochemistry, thermochemical kinetics, noncovalent interactions, excited states, and transition elements: two new functionals and systematic testing of four M06-class functionals and 12 other functionals, Theor. Chem. Acc., 120 (2007) 215-241.

[21] K. Fukui, Formulation of the reaction coordinate, J. Phys. Chem., 74 (1970) 4161-4163.

[22] K. Fukui, The path of chemical reactions - the IRC approach, Acc. Chem. Res., 14 (1981) 363-368.

[23] H.P. Hratchian, H.B. Schlegel, Accurate reaction paths using a Hessian based predictor-corrector integrator., J. Chem. Phys., 120 (2004) 9918-9924.

[24] G.W.T.M.J. Frisch, H.B. Schlegel, G.E. Scuseria, M.A. Robb, J.R. Cheeseman, G. Scalmani, V. Barone, B. Mennucci, G.A. Petersson, H. Nakatsuji, M. Caricato, X. Li, H.P. Hratchian, A.F. Izmaylov, J. Bloino, G. Zheng, J.L. Sonnenberg, M. Hada, M. Ehara, K. Toyota, R. Fukuda, J. Hasegawa, M. Ishida, T. Nakajima, Y. Honda, O. Kitao, H. Nakai, T. Vreven, J. J. A. Montgomery, J.E. Peralta, F. Ogliaro, M. Bearpark, J.J. Heyd, E. Brothers, K.N. Kudin, V.N. Staroverov, R. Kobayashi, J. Normand, K. Raghavachari, A. Rendell, J.C. Burant, S.S. Iyengar, J. Tomasi, M. Cossi, N. Rega, J.M. Millam, M. Klene, J.E. Knox, J.B. Cross, V. Bakken, C. Adamo, J. Jaramillo, R. Gomperts, R.E. Stratmann, O. Yazyev, A.J. Austin, R. Cammi, C. Pomelli, J.W. Ochterski, R.L. Martin, K. Morokuma, V.G. Zakrzewski, G.A. Voth, P. Salvador, J.J. Dannenberg, S. Dapprich, A.D. Daniels, Ö. Farkas, J.B. Foresman, J.V. Ortiz, J. Cioslowski, D.J. Fox, Gaussian 09, Gaussian, Inc., Wallingford, CT, 2009, pp. Gaussian 09.

[25] H.E. Gottlieb, V. Kotlyar, A. Nudelman, NMR Chemical Shifts of Common Laboratory Solvents as Trace Impurities, J. Org. Chem., 62 (1997) 7512-7515.

[26] SDBSWeb, Spectral Database of Organic Compounds, http://sdbs.db.aist.go.jp/sdbs/cgi-bin/cre_index.cgi (accessed 22 June 2018).

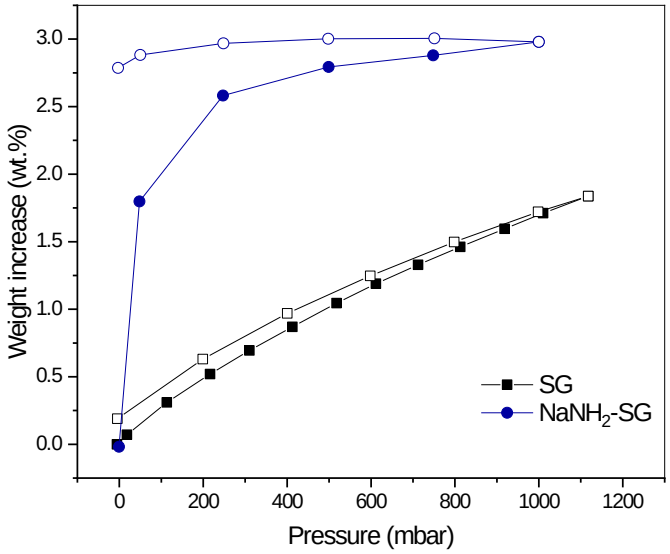
Weight increase (wt.%)
Pressure (mbar)
SG
NaNH2-SG
0.0
0.5
1.0
1.5
2.0
2.5
3.0
0
200
400
600
800
1000
1200

Figure 1

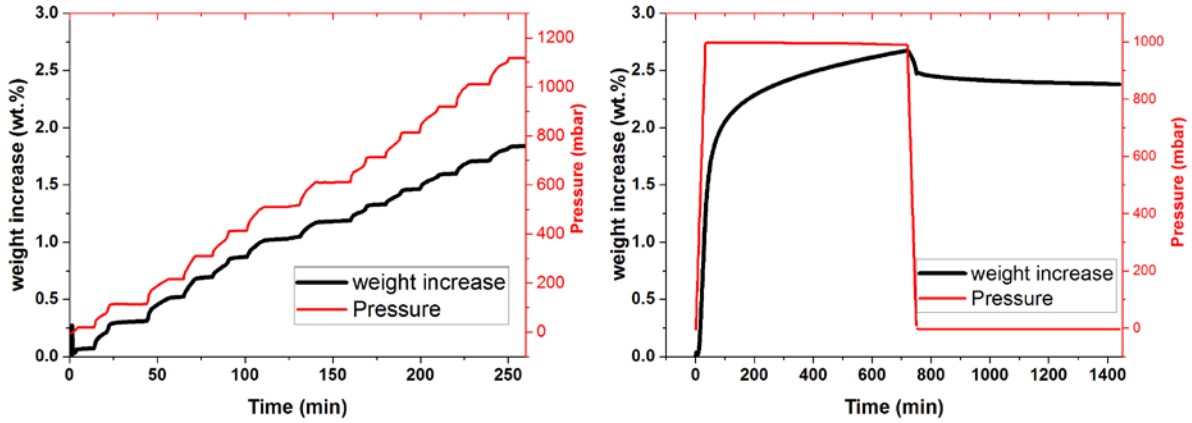
weight increase (wt.%)
Pressure (mbar)
Time (min)
weight increase
Pressure
weight increase (wt.%)
Pressure (mbar)
Time (min)
weight increase
Pressure

Figure 2

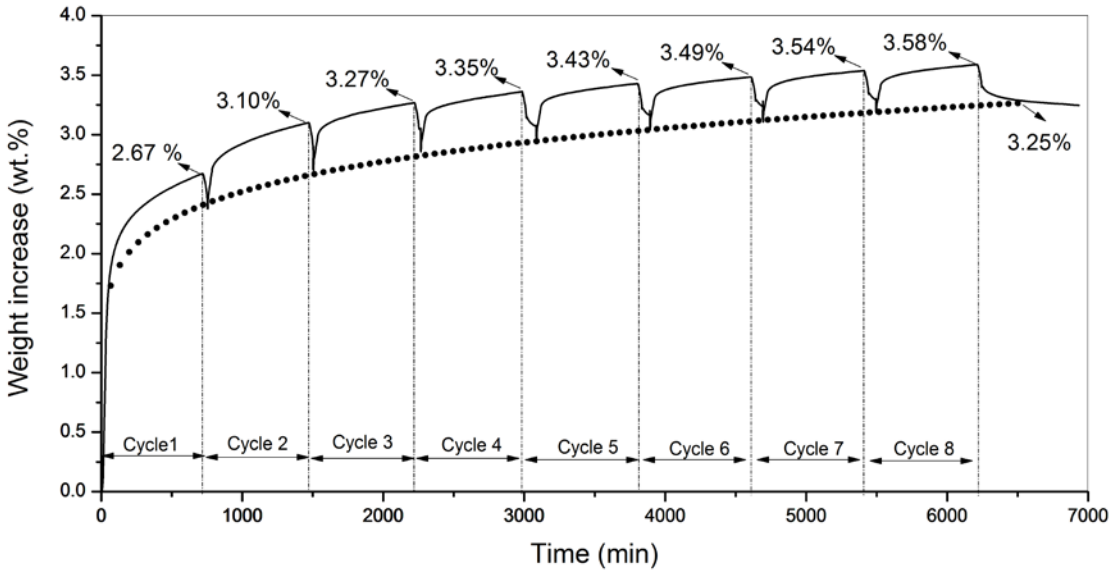
Weight increase (wt.%)
Time (min)
2.67 %
3.10%
3.27%
3.35%
3.43%
3.49%
3.54%
3.58%
3.25%
Cycle1
Cycle 2
Cycle 3
Cycle 4
Cycle 5
Cycle 6
Cycle 7
Cycle 8

Figure 3

Figure 4

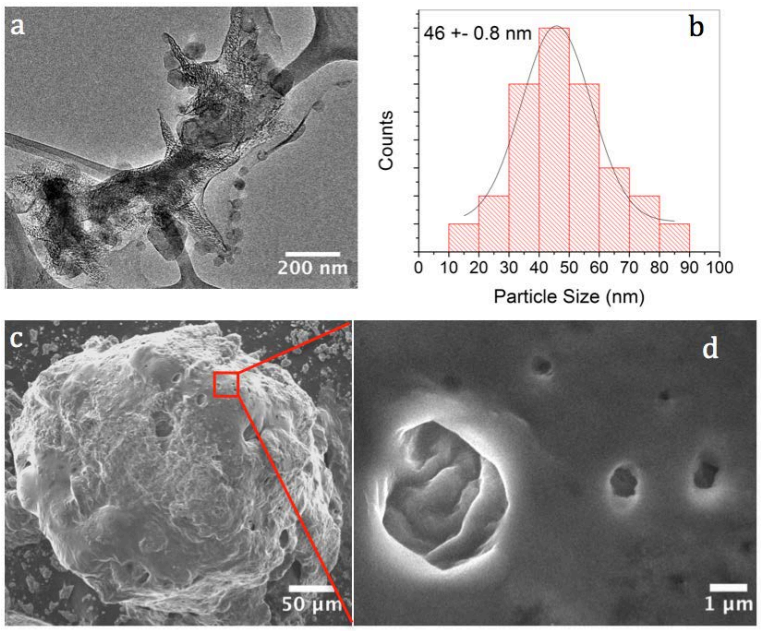
a
200 nm
b
46 +- 0.8 nm
Counts
0 10 20 30 40 50 60 70 80 90 100
Particle Size (nm)
c
50 µm
d
1 µm

Figure 5

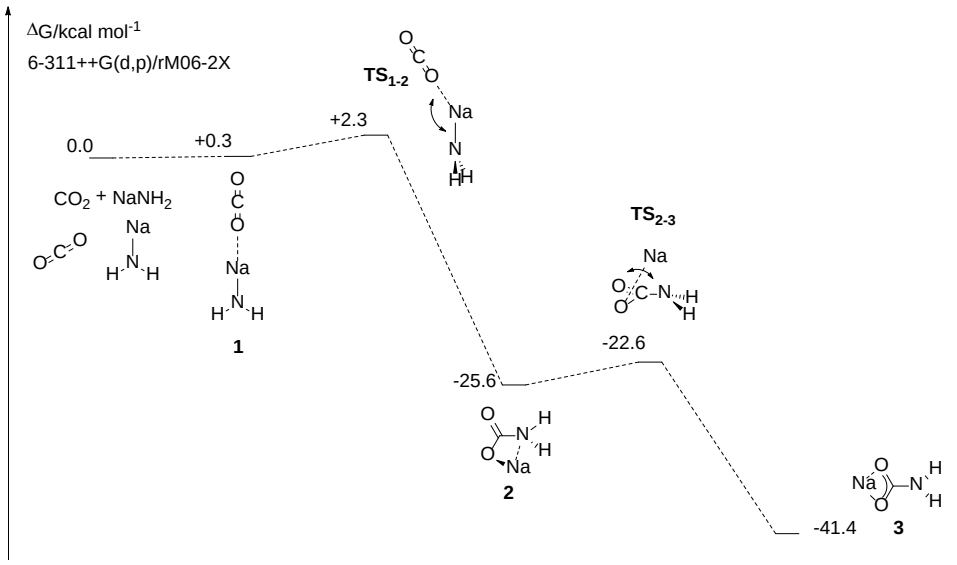
ΔG/kcal mol-1
6-311++G(d,p)/rM06-2X
0.0
+0.3
+2.3
-25.6
-22.6
-41.4
CO2 + NaNH2
TS1-2
TS2-3
1
2
3

Figure 6

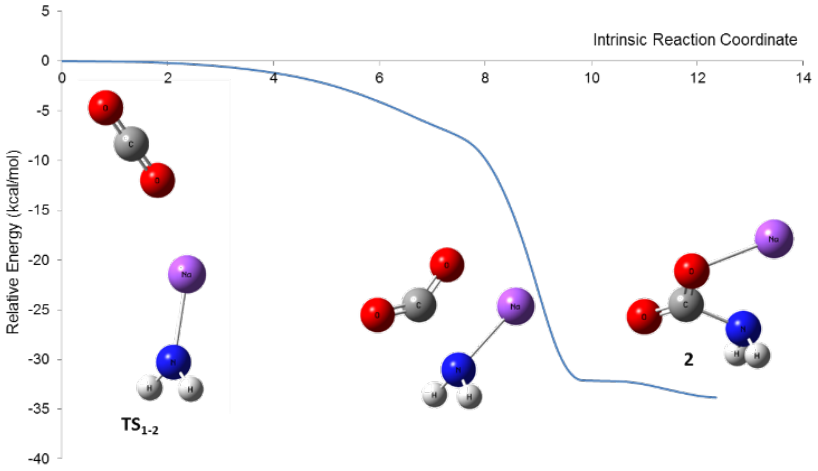
Intrinsic Reaction Coordinate
Relative Energy (kcal/mol)
5
0
-5
-10
-15
-20
-25
-30
-35
-40
0
2
4
6
8
10
12
14
TS1-2
2

Figure 7

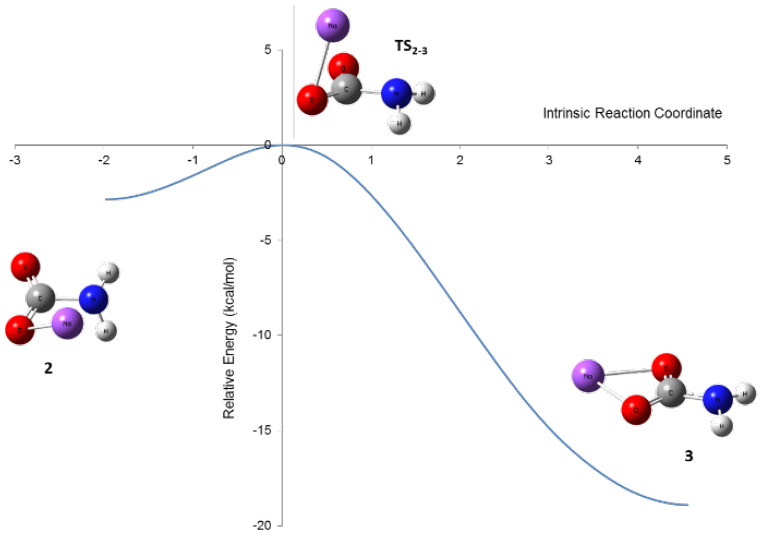
TS2-3
Intrinsic Reaction Coordinate
Relative Energy (kcal/mol)
2
3
5
0
-5
-10
-15
-20
-3
-2
-1
0
1
2
3
4
5

Figure 8

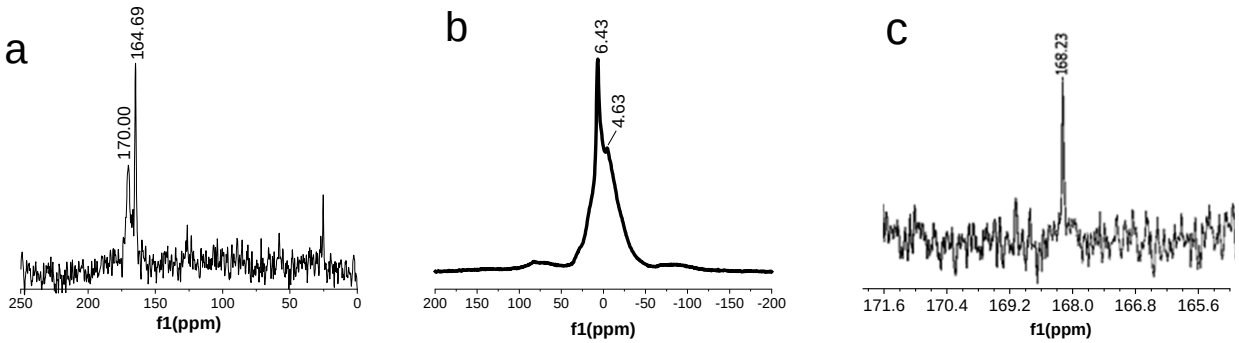
a
164.69
170.00
250
200
150
100
50
0
f1(ppm)
b
6.43
4.63
200
150
100
50
0
-50
-100
-150
-200
f1(ppm)
c
168.23
171.6
170.4
169.2
168.0
166.8
165.6
f1(ppm)

Figure 9